Article

JOURNAL OF COMPOSITE MATERIALS

Journal of Composite Materials
45(10) 1091–1107

DOI: 10.1177/0021998310389088
jcm.sagepub.com
SAGE

Investigation of the effect of single wall carbon nanotubes on interlaminar fracture toughness of woven carbon fiber–epoxy composites†

Piyush R. Thakre[1], Dimitris C. Lagoudas[1], Jaret C. Riddick[2], Thomas S. Gates[3], Sarah-Jane V. Frankland[4], James G. Ratcliffe[4], Jiang (John) Zhu[5] and Enrique V. Barrera[6]

Abstract

Single wall carbon nanotubes (SWCNTs) were introduced in the interlaminar region of woven carbon fiber–epoxy composites and the mode-I delamination behavior was investigated. Pristine (P-SWCNT) and functionalized (F-SWCNT) nanotubes were sprayed in the mid-plane of these laminates and delamination was initiated using a teflon pre-crack insert. The composite laminates were produced using vacuum-assisted resin transfer molding process. The interlaminar fracture toughness (ILFT) represented by mode-I critical strain energy release rate (G_{Ic}) for the initiation of delamination was measured using double cantilever beam tests. The specimens with pristine nanotubes and functionalized nanotubes showed a small effect on the ILFT. The specimens with P-SWCNTs showed stable crack growth and the potential for enhanced crack bridging along with slightly higher G_{Ic} than F-SWCNT specimens. Scanning electron microscopy images showed enhanced fiber–matrix interfacial bonding in the specimens with F-SWCNTs. However, large unstable crack propagation was observed in these F-SWCNT specimens from load–displacement curves and crack propagation videos. This research helps in understanding the differences in mechanisms by addition of functionalized and unfunctionalized (pristine) nanotubes to the woven carbon fiber–epoxy matrix composite laminates.

Keywords

carbon nanotubes, interlaminar fracture, delamination, carbon fiber composites, woven fabric composites, VARTM, DCB

Introduction

There has been an increase in the use of epoxy resin-based composite laminates in the aerospace industry in recent years due to their light weight, desirable mechanical properties and ability to be molded into complex shapes.[1–5] Epoxies find wide applications in composites due to their good chemical resistance and heat resistance along with good thermo-mechanical properties such as strength, elastic modulus, and glass transition temperatures, which can be tuned by adjusting chemical composition and curing kinetics[6,7] as per the desired performance requirements. However, conventional epoxies exhibit inherent brittleness and low fracture toughness, and consequently, epoxy-based laminates can be susceptible to delamination, i.e., separation between individual plies.[8–11] Increasingly demanding requirements for mechanical, thermal, and electrical properties of composite laminates have made it

† *In memoriam of Thomas S. Gates*

[1]Materials Science and Engineering, Department of Aerospace Engineering, Texas A & M University, College Station, Texas 77840, USA.
[2]Army Research Lab, Aberdeen, Maryland 21005, USA.
[3]Durability, Damage Tolerance and Reliability Branch, NASA Langley Research Center, Hampton, Virginia 23681, USA.
[4]National Institute of Aerospace, Hampton, Virginia 23666, USA.
[5]NanoRidge Materials Inc., Houston, Texas 77023, USA.
[6]Department of Mechanical Engineering and Materials Science, Rice University, Houston, Texas 77005, USA.

Corresponding author:
Dimitris C. Lagoudas, Materials Science and Engineering, Department of Aerospace Engineering, Texas A & M University, College Station, Texas 77840, USA
Email: lagoudas@tamu.edu

necessary to develop new material systems without adding weight penalties and simultaneously introducing the possibility for multifunctionality.

Recent efforts have been reported in that direction to combine the advantages of traditional advanced composites with nano- and micro-sized reinforcements to enhance thermo-mechanical and electrical properties.[12–20] Some of these efforts were directed toward resolving a critical issue in textile composites associated with the formation of matrix-rich regions in textile composites. The polymer matrix-rich region has been reported to be one of the reasons for the poor out-of-plane properties and a contributing factor to crack initiation and propagation, resulting in poor resistance to delamination growth.

In the past, particulate reinforcements have been used in composites in an effort to improve the interlaminar fracture toughness (ILFT).[12,14–17,21–25] For example, hybrid composites with alumina, silica, rubber, and glass spheres forming secondary phases in the epoxy matrix were studied by Kinloch et al.[21] It was shown that rubbery particles improved the fracture toughness of a thermosetting epoxy polymer, but reduced its strength. In fact, a combination of rubber and glass particles showed a better improvement in toughness. Sohn and Hu[22] reported improvement in ILFT with introduction of KEVLAR short fibers in fiber-reinforced polymer composites. There was little effect on the initiation toughness values, but extensive fiber bridging led to a significant increase in propagation toughness, indicating increased resistance to delamination growth. Sela and Ishai[4] reported methods for improving ILFT by introducing tough interleaves instead of particulate reinforcements and using thermoplastic matrices. Such interleaved composites showed a significant improvement in impact resistance. However, the major disadvantage of a composite with tough interleaves was shown to be the weight penalty along with low stiffness and strength of tough layers, which proportionately reduced stiffness and strength of the laminate. Thermoplastic matrices in interleaves showed an order of magnitude increase in ILFT; however, low thermal stability, interfacial wetting problems, poor chemical resistance to solvents and acids, and creep problems associated with the thermoplastic matrices limit their use in aircraft structures. Reinforcing polymer matrix-rich regions with particles or using interleaves did not provide adequate improvements in toughness and resulted in reduced strength and glass transition temperature.[7,21,22]

Carbon nanotubes have been reported to be used as reinforcement in polymer matrices due to their outstanding electrical, thermal and mechanical properties.[12–17,26–35] Extensive research has been performed in characterizing[6,28,29,33–35] and modeling[26–28,30,32,36] carbon nanotube–polymer matrix nanocomposites. One of the methods to disperse the carbon nanotube bundles and form enhanced interaction between the nanotubes and the surrounding polymer matrix has been by the process of covalent functionalization of nanotubes, which involves attaching chemical functional groups that can form bonds with the particular matrix in addition to dispersing the nanotube bundles.[14,28,33,35,37,38] The reinforcement of conventional composites with carbon nanotubes may play an important role in realizing the potential of such composites in structural applications as well as introduce multifunctional properties.

Recently, Wichmann et al.[17] reported about 16% improvement in interlaminar shear strength while the ILFT was unaffected as a result of introduction of carbon nanotubes in glass fiber–epoxy composites. The carbon nanotubes were mixed in the epoxy matrix before impregnating glass fibers to produce the laminated composite. An improvement of about 300% in mode-I ILFT was reported by Veedu et al.[16] by growing nanotubes on SiC fabric composites. Bekyarova et al.[12] reported the use of electrophoresis for selective deposition of nanotubes on woven carbon fabric. The interlaminar shear strength was improved by about 30%, along with improved out-of-plane electrical conductivity. Functionalized SWCNTs showed an improvement of about 40% in the shear strength by adding 0.5 wt% SWCNT as reported by Bekyarova et al.[13] Such efforts suggest the feasibility of improving ILFT by introducing carbon nanotubes. However, there have been several unresolved issues, such as, the addition of nanotubes to epoxy resin results in a significant increase in the viscosity of epoxy matrix leading to processing difficulties on a larger scale. Furthermore, direct mixing into epoxy resin distributes nanotubes throughout the composite laminate, reinforcing critical as well as noncritical areas and therefore leads to unnecessary cost increase. The chemical vapor deposition method to grow nanotubes on fiber preforms or fabric material could be potentially difficult to implement on an industrial scale.

As an alternate approach, we propose in this study to use nanotubes in small quantities at critical regions, i.e., at the interfaces susceptible to delamination. The objective of this article is to understand the influence of such selective reinforcement of carbon nanotubes on the mode-I ILFT of woven carbon fiber–epoxy composites processed using vacuum-assisted resin transfer molding (VARTM) technique. A novel spraying technique was used for the selective placement of nanotubes without increasing the viscosity of the epoxy matrix. The spraying process is easier to scale-up to the industrial production and ensures limited use of carbon nanotubes only in the susceptible areas.

Several panels were processed using VARTM method incorporating functionalized as well as unfunctionalized (pristine) carbon nanotubes.

The VARTM process has been chosen as it is widely used for applications in commercial, military, and aerospace composite structures. One of the advantages of the VARTM process is that it is easier to scale up to industrial production. For a successful application, the matrix properties which govern processing characteristics like viscosity must be considered in addition to meeting the requirements for mechanical properties in service. A number of low-viscosity epoxy resins have been developed to meet the processing requirements associated with the VARTM. An epoxy with room-temperature curing agent was selected for this study on the basis of lowest viscosity for easier VARTM processing. The nanotubes were functionalized for better dispersion in the epoxy matrix along with enhanced compatibility with epoxy through better bonding characteristics. The presence of nanotubes on the intended region of the laminate, after VARTM processing, was confirmed from the microscopy images.

The mode I ILFT, G_{Ic}, of the laminates considered in the current study was characterized using the double cantilever beam (DCB) test. This test was conducted in accordance with the guidelines contained in the ASTM International Standard, D5528-01.[39] The major exception in the current study to the guidelines of D5528-01 was that the DCB specimens were made from fabric. Similar tests conducted on either textile or fabric-based laminates have been reported previously. Choi et al.[11] and de Morais et al.[40] have studied the delamination resistance of multidirectional composites and reported higher values for ILFT as compared to unidirectional composites. The delamination resistance of unidirectional and plain weave fabric IM7/8552 was compared by Paris et al.[41] using the DCB test. The average value of initiation G_{Ic} of the fabric IM7/8552 was reported to be 263 J/m^2.[41] This value is only 3% greater than the initiation G_{Ic} value reported by Hansen and Martin[42] of tape IM7/8552. Although the coefficient of variation was higher for the fabric specimens reported by Paris,[41] this similarity in initiation values of G_{Ic} suggests that reliable values of initiation G_{Ic} may be obtained from DCB tests conducted on fabric material systems.

In short, a novel method for selective placement of carbon nanotubes in woven carbon fabric composites is presented in this article, along with the characterization results for mode-I ILFT using DCB tests and fracture mechanisms using scanning electron microscopy (SEM). The DCB specimen preparation, test methods, and data reduction methods are described in section 'Experimental methods', preceded by the material description and processing technique in section 'Materials'. The results of DCB data analysis are discussed in the sections 'Force–displacement response' and 'ILFT measurements'. Post-delamination fracture surfaces were studied using SEM as described in section 'Mechanisms of delamination: SEM fractography', followed by summary of this study in the last section.

Materials

The purified single wall carbon nanotubes (SWCNTs) were obtained from Rice University, and were made by the high pressure carbon monoxide synthesis process (HiPCO). The supplied material consisted of micron-scale aggregates with individual SWCNT diameters reported to be 1.0–1.4 nm. Functionalized nanotubes were prepared through a three-step chemical treatment. The carbon nanotubes were first fluorinated in a Monel flow reactor at 150°C for 12 h following the procedure developed at Rice University.[38] Hydroxylated nanotubes were then prepared through reaction of the fluoronanotubes with lithium hydroxide treated ethyleneglycol.[35] Finally, the organosilane N-(2-aminoethyl)-3-aminopropyltrimethoxysilane obtained from Aldrich Inc. was used to produce silane functionalized nanotubes. This procedure has been demonstrated in previous work to successfully functionalize nanotubes with organosilanes.[38] For spraying the nanotubes onto the carbon fabric plies, a solution was prepared using 0.1 wt% purified pristine nanotubes in ethanol, and another solution was prepared using 0.1 wt% silane functionalized nanotubes in ethanol. The 0.1 wt% represents weight fraction with respect to weight of an individual ply of woven carbon fibers. The total weight fraction of carbon nanotubes amounts to be 0.01 wt% of the total weight of all plies.

The epoxy resin used was diglycidyl ether of bisphenol-F (DGEBF) epoxy EPON 862 (now called EPIKOTE 862), and was obtained from Resolution Performance Products along with aliphatic amine curing agent EPICURE 9553. The low viscosity makes this epoxy suitable for VARTM process and therefore eliminates the use of viscosity reducers and reactive diluents from the epoxy formulation.

The woven carbon fabric used in the composite was an eight-harness satin weave (8 H.S.) of T300 carbon fibers produced by Textile Technologies Incorporation. NASA Langley Research Center (LaRC) provided the woven fabric in the form of a roll of 12 in. (30.5 cm) wide and about 40 ft (1220 cm) long.

The VARTM process was used to fabricate laminate plates using the mold set-up as shown in Figure 1, and detailed information about the VARTM processing and the nanotube spraying method has been provided in reference.[14] Each panel contained 10 layers of carbon fabric plies and carbon nanotubes were sprayed at

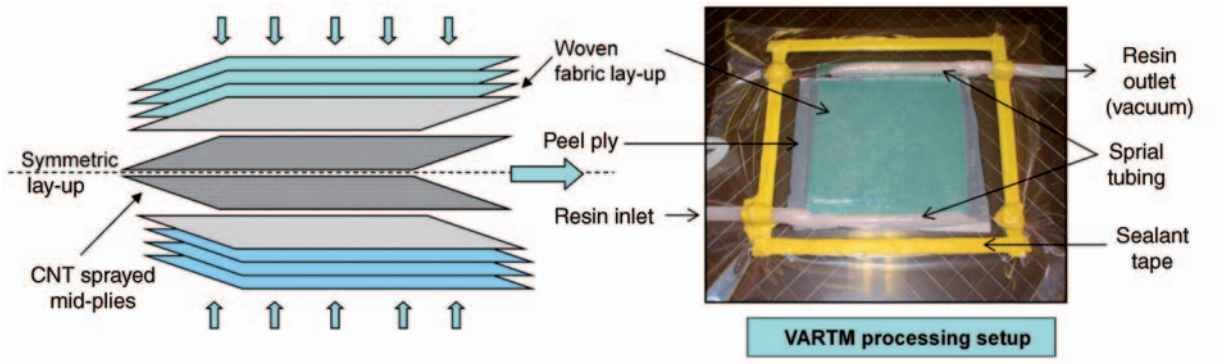

Figure 1. Schematic representation of ply lay-up and actual VARTM process.

Table 1. Composite panels prepared by the VARTM technique and their nomenclature

Panel number	Mid-plane modification	Specimens (6 each)
P1	No nanotubes, solvent evaporated	1P1 to 6P1
P2	0.01 wt% pristine nanotubes	1P2 to 6P2
P3	0.01 wt% silane functionalized nanotubes	1P3 to 6P3

the mid-plane of the laminate (i.e., between ply numbers 5 and 6). The ply stacking was kept symmetric about the mid-plane as shown in Figure 1. A polytetraflouro ethylene (PTFE) film insert of size about 3 in. wide (7.62 cm) and 8 in. long (20.32 cm) was placed at the mid-plane of the fiber stack as the delamination starter material. Three different panels were processed as described in Table 1, each of dimensions approximately 8 in. (20.32 cm) wide, 6 in. (15.24 cm) in length and about 0.16 in. (0.40 cm) in depth after removing the rough edges from four sides. The measurements were performed with an accuracy of 0.1 mm (0.004 in.) in width and 0.01 mm (0.0004 in.) in thickness. The nomenclature for the DCB test specimens consisted of the panel number preceded by the specimen number, e.g., 5P2 indicates 5th specimen of the 2nd panel. The numbering of specimens from 1 to 6 indicates cutting direction from left to right in the panel, i.e., specimen 1 and 6 forming the edge specimens.

Experimental methods

Specimen preparation

The specimens were cut according to ASTM-5528 standards with length of 6 in. (15.24 cm) and width of 1 in. (2.54 cm) with an accuracy of ±0.1 mm. The upper and lower specimen surfaces were roughened using grinding article where the piano hinges were to be bonded. The surfaces of the piano hinges were sand blasted to prepare rough surfaces for better bonding, and then the surface was cleaned with acetone to remove any contamination. The specimens were dried for 4 days at 60°C in a Thermolyne Oven (Series 9000) to remove moisture absorbed during the cutting process. Two-part epoxy adhesive was used to bond the piano hinges, and the specimens were placed in an oven for 2 h at 60°C to cure the epoxy adhesive. The specimen edges were sprayed with white paint, and a scale with 1 mm resolution was placed on one of the edges of each specimen for monitoring crack propagation, as shown in Figure 2(a). The specimens were stored in a desiccator before testing to protect them from humid conditions and also after testing to preserve the fracture surfaces for microscopic investigation.

Double cantilever beam test

The ASTM D-5528 standard was followed for performing the DCB tests at room temperature using a servo-hydraulic test frame (MTS 858 table top system) as shown in Figure 2(b). A 50 lbf (222.50 N) load cell with ±0.05 N resolution (interface model 1500 ASK-50) was used for force measurement. Parameters P, δ , and a represent force, applied displacement, and delamination length, respectively. Crack propagation was monitored on a video screen connected to a video camera set at a magnification of about 20× and focused on the crack tip at all times as the crack progressed. The test was conducted under displacement control at a displacement rate of 1.27 mm/min. Crack extension was recorded every millimeter of crack growth for stable crack growths, and crack propagations corresponding to start and end values of unstable crack growths were noted. The crack was allowed to propagate through a distance of at least 40 mm, after which the specimen was unloaded at a rate of 2.54 mm/min.

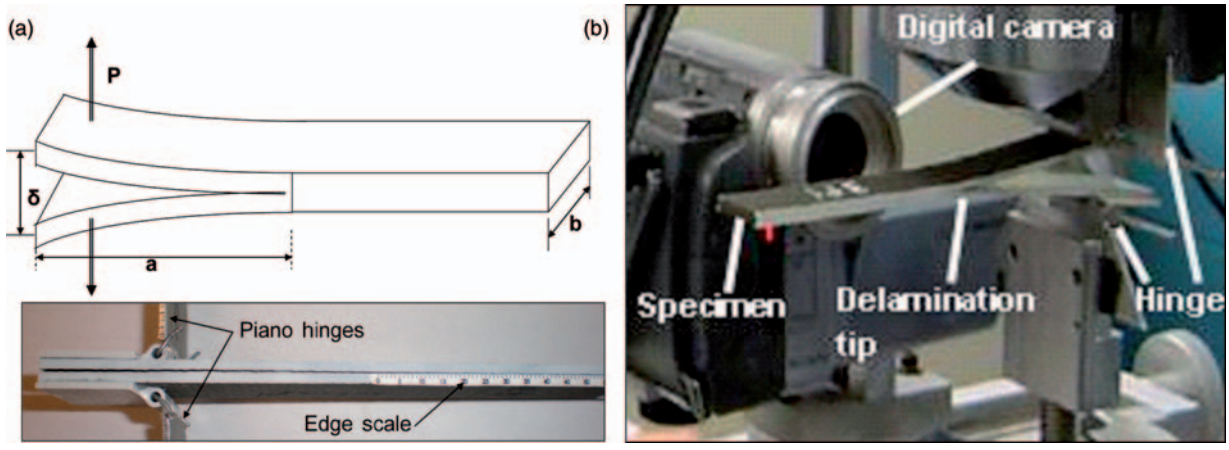

Figure 2. Double cantilever beam test: (a) specimen specifications and (b) test set-up.

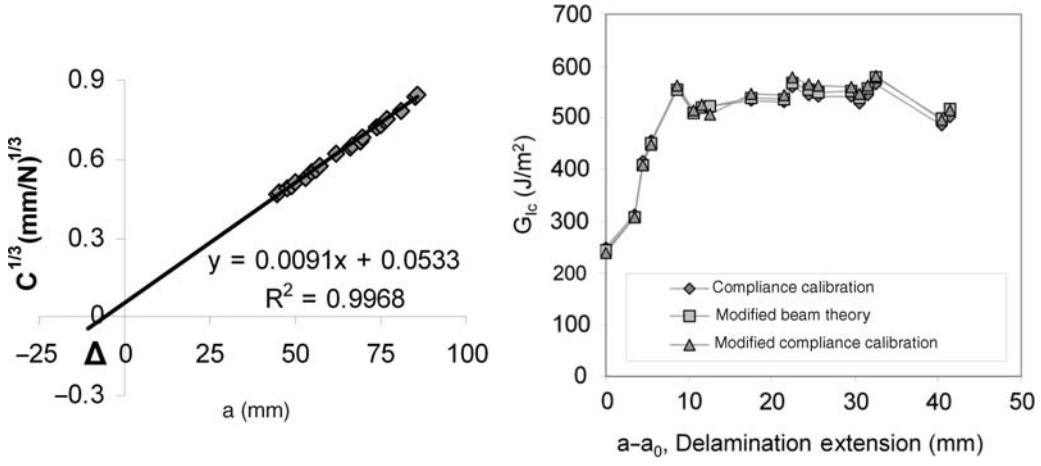

Figure 3. Data reduction method: (a) Method to find the correction factor, Δ, x-intercept value obtained by extending the straight line through the data points. (b) Comparison of R- curves from three data reduction techniques (CC, MBT and MCC) for one representative specimen 1P2.

Data reduction method

Three data reduction methods (i.e., and the modified beam theory (MBT), the compliance calibration (CC) and the modified compliance calibration (MCC)[39]), were utilized to calculate the G_I values i.e., strain energy release rates. A comparison of the results is shown in Figure 3(b) for a sample specimen using the three different techniques of data reduction, as per the ASTM standards. Figure 3(b) shows almost overlapping R-curves from all three methods. Further comparison of the results for different specimens has been presented using only the MBT.

Modified beam theory. In the MBT method, each arm of the DCB specimen is considered to be a cantilever beam of length equal to the delamination length 'a'. The G_I value calculated by Euler–Bernoulli beam theory is overestimated in the absence of perfectly clamped delamination front as shown by Hashemi et al.[43] Thus to correct for this nonperfect clamping effect, Hashemi et al. suggested a slightly longer delamination length, $a+\Delta$, where Δ is determined from the plot of the cube root of compliance, $C^{1/3}$, vs. delamination length, 'a' as shown in Figure 3(a). The compliance, C, is the ratio of load point displacement to the applied load, i.e., $C=\delta/P$. The strain energy release rate is calculated by using Equation (1) as follows:

$$G_I = \frac{3P\delta}{2b(a+\Delta)} \tag{1}$$

where P is the applied load for crack growth, δ the corresponding load point displacement, 'a' the corresponding delamination length (or initial crack length), b the specimen width, and G_I the strain energy release

rate (G_{Ic} is the critical value known as mode-I ILFT and is considered to be a material property of the particular composite). The analysis method required the measurement of only three parameters, i.e. P, δ and 'a' during the test, and Δ was obtained using the method suggested by Hashemi et al.,[43] as shown in Figure 3(a).

Scanning electron microscopy

A Hitachi S-3700N scanning electron microscope was used for studying the delaminated fracture surfaces of the DCB specimens, and imaging was performed using Oxford Instruments INCAx-Sight Model 7962. The specimens were split open after completion of the DCB test and the mid-planes were coated with a 2-nm thick platinum layer to reduce the charging effect of the specimen surface under the electron beam. The specimens were imaged at different locations along the crack length as shown in Figure 4, to maintain consistency in comparison for specimens from different panels.

Results and discussion

Force–displacement response

The comparison of the delamination initiation and the delamination propagation as observed from the force–displacement curves is shown in Figure 5(a) for representative specimens taken from the same area of the laminate from three different panels. The large unstable delamination growth behavior identified by a sudden drop in force (more than 50% of the peak force) from point A to B, as shown in Figure 5(a), was observed only in the panel with functionalized nanotubes. The force drop results from a delamination

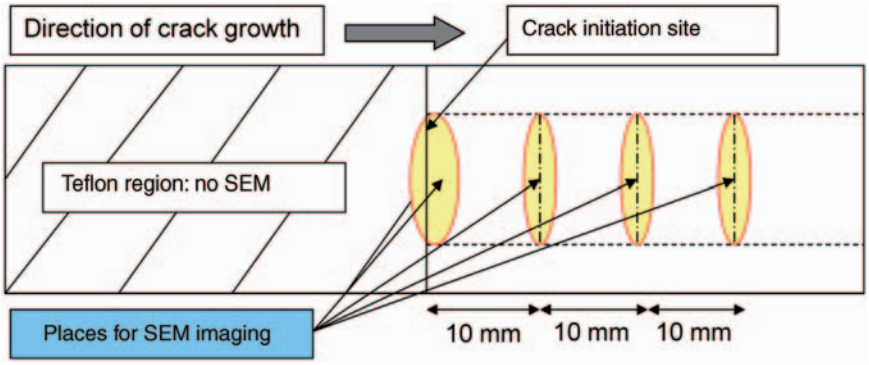

Figure 4. SEM locations along crack length for consistency of comparison between specimens from different panels. (Not drawn to scale. Actual specimen length 16 cm and width 2.5 cm).

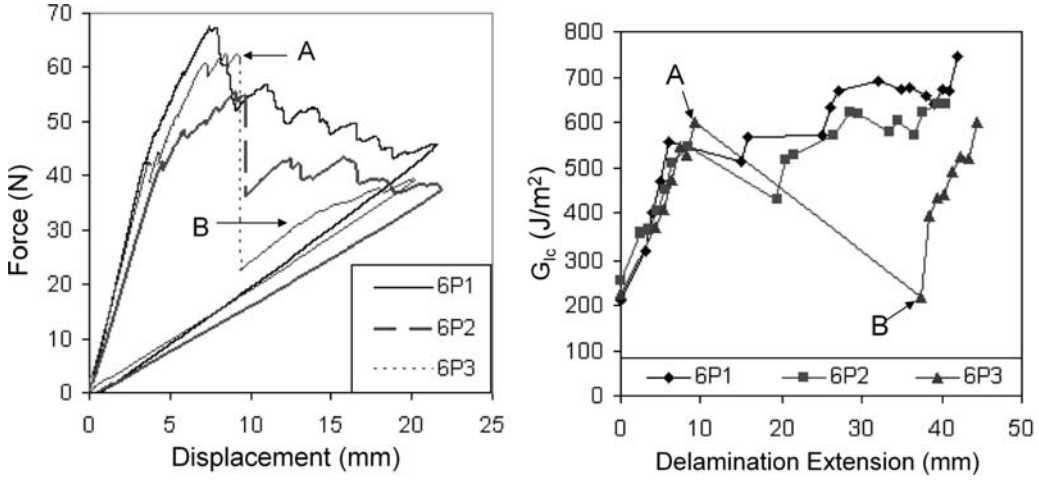

Figure 5. Representative graphs for one specimen each from three panels: 6P1–no nanotubes, 6P2–Pristine nanotubes, 6P3–Functionalized nanotubes; (a) force–displacement curves and (b) R-curves (resistance curves).

extension of about 30 mm (point A to B) as seen from Figure 5(b). Usually, the unstable delamination growth behavior shows about 3–5 mm delamination extension[41,44] resulting in about 8–15% drop from the peak force. The reasons for the large unstable delamination growth behavior in the specimens with functionalized nanotubes have been discussed in section 'ILFT measurements'.

Figure 6 shows the force–displacement curves for six specimens from individual panels along with the average force–displacement curve (shown by a dark curve) for that particular panel. The initial response for all specimens was linear until the delamination initiation. The linear response was followed by a combination of stable and unstable delamination growths. The stable response was represented by a gradual decrease in force with delamination growth. The unstable response has been characterized by sudden drop in force with delamination growth. Figure 6(a) shows gradual decrease in force with increasing load–point displacement for all specimens from panel P1 (base laminate with no nanotubes). The difference (33%) in slope of the linear region for specimen 6P1 is due to the difference in initial delamination length which was about 6 mm shorter as compared to the average of the rest of the specimens. The slope of the linear regions overlapped for all specimens from panel P2 (pristine nanotubes). Specimen 5P2 seems to be an outlier as it is the only specimen showing large force drop (50%) out of total six specimens. From Figure 6(c), the difference in the slope of the linear region between specimens 1P3–2P3 and specimens 3P3–6P3 is largely due to the difference in initial delamination lengths. A difference of around 2.5 mm in initial delamination lengths resulted in about 17% difference in slopes. If the displacement is normalized with respect to initial delamination length ($\delta/(a_0)^3$) for the linear region then the effect of 'a' disappears from the linear slope. Large force drops (50–70%) were consistently observed in all specimens with functionalized nanotubes, as shown in Figure 6(c). As can be seen from Figure 6(c) and Figure 6(d), large unstable delamination growth represented by force drops of about 30–40 N was the characteristic behavior of the panel with functionalized nanotubes as observed from the

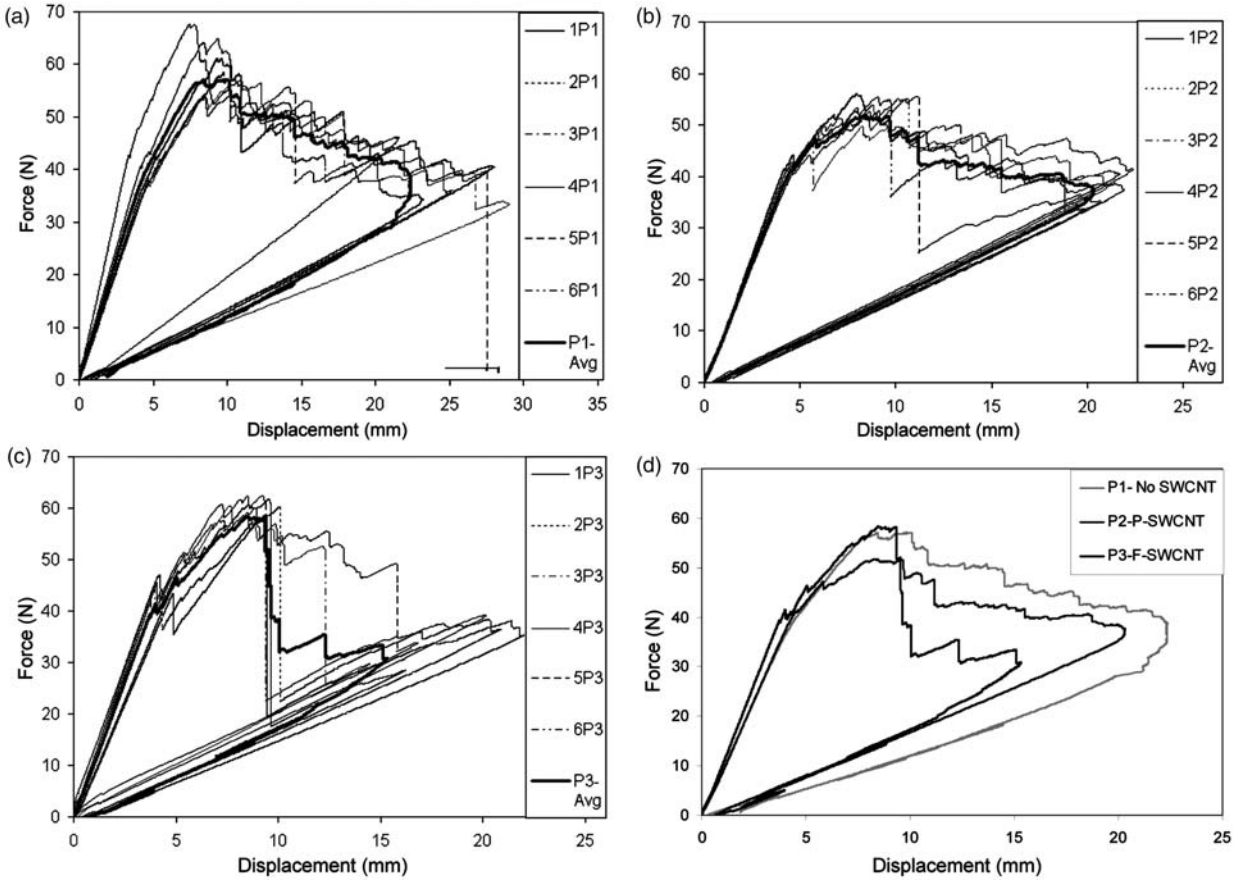

Figure 6. Force–displacement curves for all panels; (a) P1: No-SWCNT, (b) P2: Pristine SWCNT, (c) P3: functionalized SWCNT, and (d) average curves.

large force drops. The average drop in force is about 50% of the peak force as shown in Figure 6(d) for the specimen with functionalized nanotubes. The average initial delamination length for the panel with functionalized nanotubes was 46 mm and for the panel without nanotubes was 46.5 mm. A small difference of 0.5 mm in initial delamination lengths resulted in about 12% difference in slopes of the linear region of average force–displacement curve and about 5% difference in slopes if the displacement is normalized with delamination length. The slope is also a function of the cube of the arm thickness, along with other differences such as specimen width, arm modulus, fiber volume fraction which can cause the difference in the initial slopes.

An increase of about 6% is found in the average delamination initiation force for the panel with pristine SWCNTs over the panel without SWCNTs (with 2% coefficient of variation). The increase in case of the panel with functionalized SWCNTs is about 14% over the panel without any nanotubes, having about 5% coefficient of variation. The coefficients of variations are very small compared to values in the literature[16,25,31,41,45,46] (about 10–15%) indicating consistency in the processing technique and repeatability of the testing method.

The area under the force–displacement curve represents energy absorbed during the overall delamination growth. Figure 6(d) represents comparison of the average of the force–displacement behavior for all panels. The area under the curve for panel with functionalized nanotubes is the lowest followed by panel with pristine nanotubes and panel without nanotubes showed comparatively largest area under the curve. This observation is consistent with the R-curve behavior discussed later in this section, which shows the lowest propagation G_{Ic} for panel with F-SWCNTs followed by panel with P-SWCNTs and the highest propagation G_{Ic} for panel without nanotubes.

The delamination initiation is followed by a small sudden drop in force for all specimens. The delamination growth was visually observed at this point from the edge of the specimen thus releasing the stored energy to create new fracture surfaces. For all specimens, the initial small force drop or variation from linearity (i.e., change in slope) was followed by an increase in force till a peak. The increase in force corresponds to the presence of fiber bridging, yarn bridging, ply bridging or a combination of these mechanisms as observed in Figure 7. Similar characteristics were observed in woven composites by Paris et al.,[41] Alif et al.[44] and Martin[47] and is termed 'ratchetting' by Martin.[47] The ratchetting of the force–displacement curve represented stick-slip propagation of the crack. The slip portion on the force–displacement response represents the delamination growth until the delamination comes to an arrest. The stick portion of the force–displacement response corresponds to fiber/yarn bridging mechanisms observed from the edge of the specimen. Sometimes, an additional delamination appeared in the front of the existing delamination, tip as shown in Figure 7(a), and grew backward around the transverse yarn. On other occasions, delamination appears to be on an adjacent plane as shown in Figure 7(b). Similar observations were made by O'Brien et al.[41] and Alif et al.[44] The stick portion was followed by a slip portion on the force–displacement curve represented by sudden drop in force (unstable crack growth). The slip portion of the force–displacement curve corresponded to the breakage/pullout of the bridging fibers or tows in the delamination plane (Figure 7(d)) or debonding of the transverse yarns as shown in Figure 7(c). Such features from Figure 7 represent some of the mechanisms

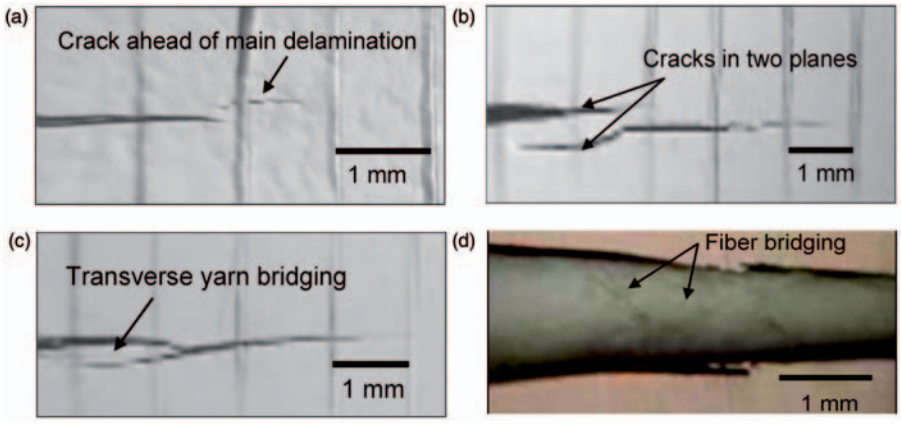

Figure 7. Crack propagation mechanisms; (a) crack initiation in front of crack tip, (b) cracks in two planes, (c) transverse yarn bridging, and (d) fiber bridging.

of energy dissipation. The images from Figure 7 are taken from representative specimens from all panels and such features were common in specimens from all panels irrespective of its constitution, i.e. irrespective of the presence or absence of nanotubes. The delamination extensions corresponding to slip portion were about 2–7 mm for the panel without nanotubes (Figure 8) and the panel with pristine nanotubes (Figure 9), which is quite similar to that observed in woven composites.[41] However, large slip behavior with corresponding delamination extension of 20–30 mm was observed in specimens from the panel with functionalized nanotubes (Figure 10).

It is important to point out that all three panels (P1, P2, and P3) from a single batch were processed together at the same time under exactly same processing conditions in the same VARTM set-up. Similar processing conditions were also maintained for the second batch of all three panels. The large stick-slip behavior (20–30 mm crack growth) was observed in most of the specimens from the panel with functionalized nanotubes, and from that panel only. Hence, it is indicated that this behavior has some relationship with functionalization of the nanotubes, and not with the processing conditions, since those were maintained consistently for all panels. It is discussed further in the section with respect to the observed delamination fracture surfaces by using SEM fractography.

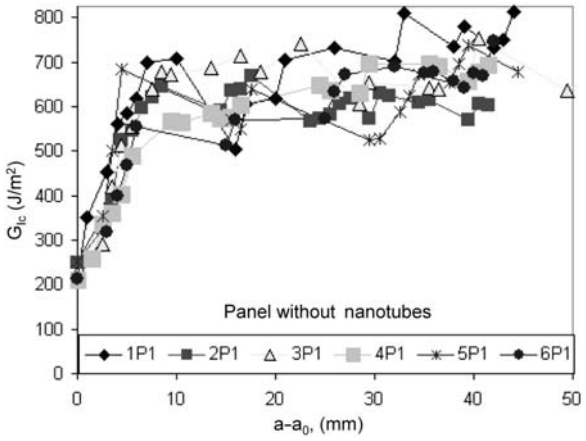

Figure 8. R-curves for six specimens from panel without any nanotubes (P1).

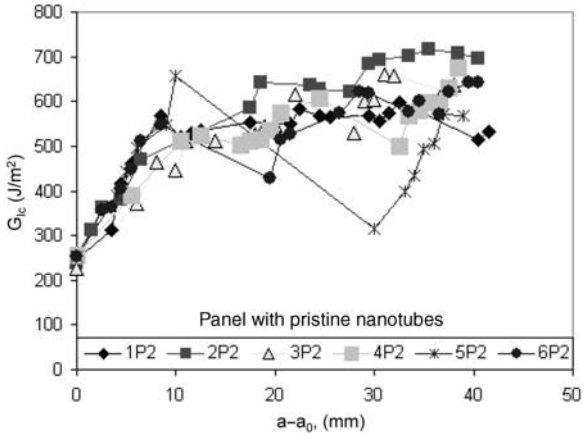

Figure 9. R-curves for six specimens from Panel 2 with pristine SWCNTs (P2).

ILFT measurements

The delamination extensions were noted from a marked scale on the edge, with 1 mm markings during various increments of stable delamination growth. In cases where growth was unstable, the delamination length corresponding to the beginning and end of the unstable period were recorded.

R- curves for all tested specimens are shown in Figures 8–10. These curves show the change in the strain energy release rate of the specimen as the initial delamination starts growing from the end of a PTFE insert and propagates through the specimen. A nonlinearity criterion is used to calculate the initiation values for the critical strain energy release rates, which are considered as the ILFT values for different laminates. According to the nonlinearity criterion,[41] force and displacement values corresponding to first deviation from linearity on the force–displacement curve is considered as the critical values for initiation of delamination growth.

The average values of initiation G_{Ic} for six specimens from each panel are presented in Table 2. The results show a 6% increase in average initiation G_{Ic} for the panel with pristine nanotubes over the panel without any nanotubes. This difference lies just beyond the

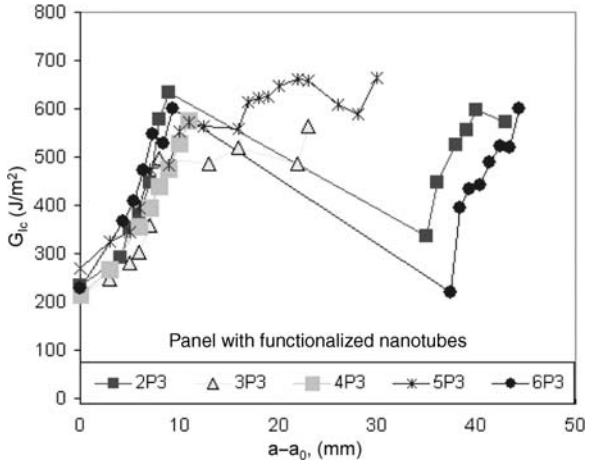

Figure 10 R-curves for six specimens from Panel 3 with functionalized SWCNTs (P3).

coefficient of variation of initiation values of G_{Ic} for the specimens with pristine nanotubes. This suggests some statistical significance to the observed increase in initiation G_{Ic} of the specimens containing pristine nanotubes. The corresponding increase in average initiation G_{Ic} for the panel with functionalized nanotubes is negligible over the panel without any nanotubes with about 8% coefficient of variation which is still lower than the reported coefficient of variation (around 14%) in literature by Martin,[47] Choi et al.[11] and Paris et al.[41]

R-curves for all specimens from the panel without nanotubes are shown in Figure 8. It shows that the G_{Ic} increases for about 7–10 mm of delamination growth, after which it plateaus and the delamination continues with small stable and unstable growths without significant increase or decrease in G_{Ic} values. Similar behavior was also observed for the panel with pristine nanotubes as shown in Figure 9. The initial increase in the G_{Ic} before the plateau has been due to the fiber bridging mechanisms. The small drop after the peak G_{Ic} was observed due to breaking of bridging fibers.

Figure 10 shows that the G_{Ic} increases almost linearly until a sudden drop in G_{Ic} with very large delamination extension. The delamination extension of about 20–30 mm was observed for five specimens out of total six specimens. For two specimens, the G_{Ic} starts to increase again after large delamination extension. In other specimens, the specimen length was not sufficient to be able to again notice the stable delamination extension. Such peculiar behavior of large delamination extension could be due to many reasons such as inhomogeneous distribution of nanotubes on the plane of lamina, smaller aspect ratio of nanotubes, suppression of fiber bridging mechanisms due to smaller length of nanotubes, etc. Tong et al.[48] presented numerical results revealing that the nanotube's length, density, and maximum pull-out displacement as well as the interfacial friction shear stress are important parameters affecting the delamination toughness. Especially, the ILFT might reduce with shorter length nanotubes. The fiber bridging mechanisms would also be suppressed due to shorter nanotube lengths. Smaller nanotubes also creates a possibility for the nanotubes to escape from the mid-plane to the adjacent planes of plies during the VARTM process resulting in poor distribution in the mid-plane resulting in observed large unstable crack growths. The average R-curve behavior for all specimens from three distinct panels is shown in Figure 11. Values of G_{Ic} for every 2 mm of delamination extension were averaged for each panel and the average G_{Ic} data points were plotted. Polynomial curve fitting was utilized to fit these data points to get the average R-curve response for each panel.

The purpose of plotting average G_{Ic} values was to compare the general trend of crack growth in different panels. It has been seen from Figure 11 that initiation G_{Ic} values for all the panels were very similar. However, propagation G_{Ic} values have been found to be lower for the panel with pristine nanotubes compared to the base laminate panel without nanotubes, and the plateau represented stable propagation unlike the curve for the panel with functionalized nanotubes.

The large unstable crack propagation behavior has been observed by the absence of a plateau in the propagation region for the panel with functionalized nanotubes, as shown in Figure 11. The propagation G_{Ic} value was not possible to calculate for this panel due to the large unstable crack propagation, and hence, insufficient number of data-points. However, the peak G_{Ic} value for the panel with F-SWCNTs has been observed to be close to the propagation value for the base laminate panel and higher than the panel with P-SWCNTs. This indicates a possibility of achieving improvement in propagation G_{Ic} for the panel with F-SWCNTs compared to that with P-SWCNTs, provided the delamination propagation can be stabilized.

Table 2. Average G_{Ic} at delamination initiation for woven carbon fiber reinforced polymer composites

Panel number	G_{Ic} initiation (J/m^2)	CoV (%)
P1: No SWCNT	230.5	8
P2: Pristine SWCNT	245 5	5
P3: Functionalized SWCNT	231.8	9

Mechanisms of delamination

Microscopic investigation of the delaminated surfaces was performed using SEM and transmission electron

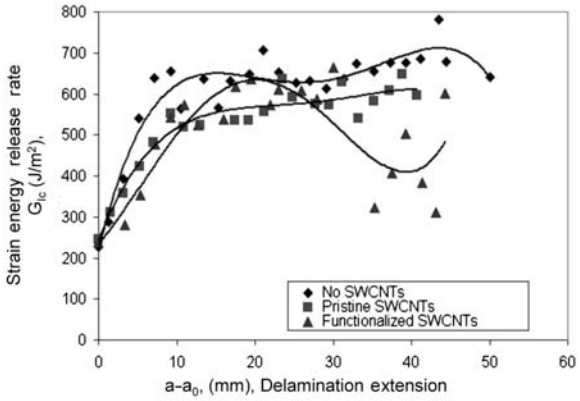

Figure 11 R-curves indicating average G_{Ic} values calculated per 2 mm of crack extension and curve fitting through average G_{Ic} indicating trend of crack growth for each panel.

microscopy (TEM) for understanding the mechanisms of crack initiation and propagation.[40] Figure 12 shows the TEM micrographs of pristine and silane functionalized nanotubes. Pristine nanotubes consisted of an agglomeration of nanotubes resulting from Van der Waals interaction resulting in larger bundle diameters. The functionalization process resulted in better dispersion with smaller nanotube bundle diameter and shorter lengths, in addition to better bonding with epoxy matrix.[33,35]

SEM images were taken at various low and high magnifications such as 20×, 100×, 5000×, and 10000× at the locations shown in Figure 4, distanced from the starter crack (end of PTFE insert). SEM images are included for samples 1P2 and 2P3, as a representation of samples with pristine nanotubes and functionalized nanotubes, respectively. The results will be presented first for the sample with pristine nanotubes at low then high magnification, followed by results for the sample with functionalized nanotubes also at low then high magnification.

Figure 13(a) and (b) includes the SEM images at low magnification of the crack initiation for the 1P2 sample. Figure 13(a) shows mostly carbon fibers in fill yarn while Figure 13(b) shows carbon nanotube network at the delamination initiation site and also on fiber-matrix

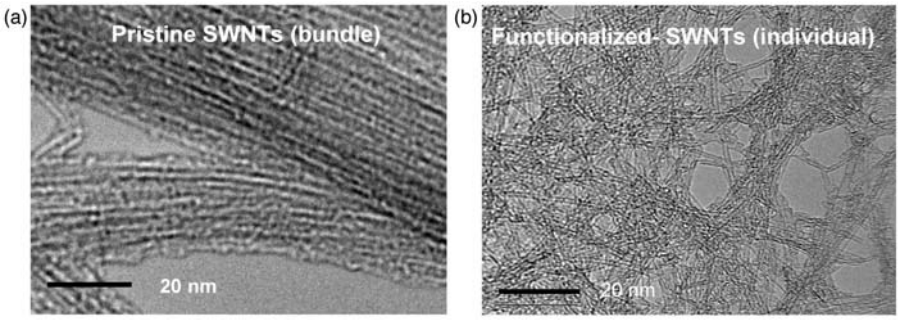

Figure 12 TEM images showing: (a) pristine SWCNTs and (b) functionalized SWCNTs.

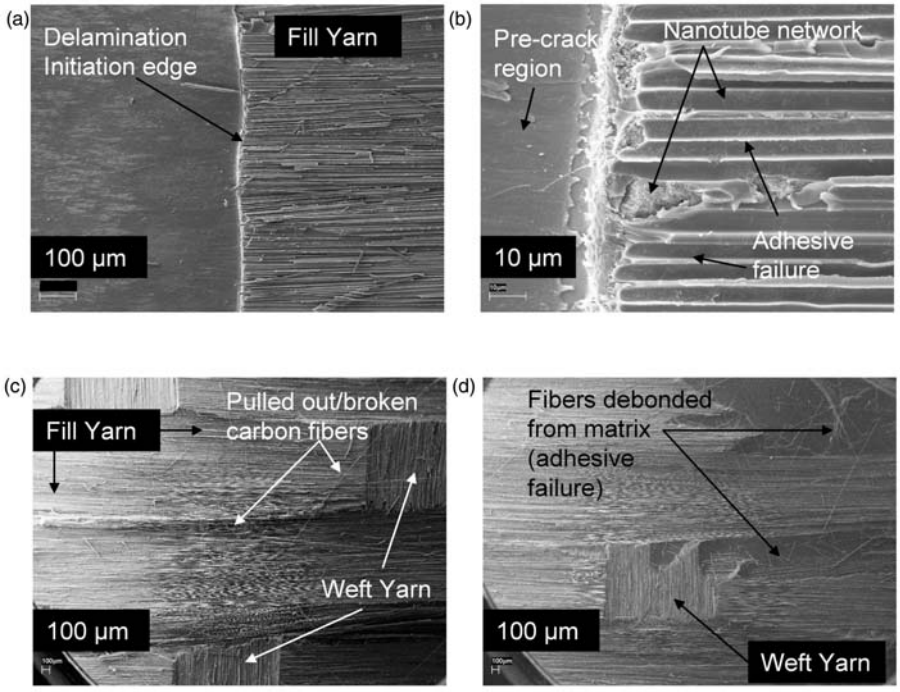

Figure 13. Low magnification SEM images of the delamination surface from the panel with pristine SWCNTs: (a,b) 0 mm (delamination initiation), (c) 20 mm from delamination initiation, (d) 30 mm from delamination initiation.

debonded surfaces. A few fibers can be seen pulled out or broken and fill/weft yarns are also seen without matrix coating. Figure 13(c) and (d) shows the SEM images at 20 and 30 mm from the delamination initiation. The pattern is very similar to that of the delamination edge marking consistent behavior over the delamination process. These images point to adhesive failure (i.e., and failure of adhesion at fiber–matrix interface), in which there is a relatively clean separation between the fiber and the matrix.

Figure 14 shows the surfaces of specimen 1P2 at high magnification. These images show the presence of nanotube bundles on the fabric surface in the form of a network distributed over the fabric surface. The nanotubes form a network which is visible at both the carbon fiber surfaces and on the carbon fiber impressions as shown in Figure 14(a) and (b), respectively.

The presence of nanotubes on the carbon fibers (Figure 14(a)) and the carbon fiber impressions on matrix (Figure 14(b)), and the absence of a continuous matrix layer covering these carbon fibers indicate fiber–matrix debonding, further supporting that adhesive failure is the key contributor to the delamination mechanism. However, the presence of long nanotubes of about a micron to few microns also indicated potential for fiber bridging and crack bridging mechanisms that could contribute to an increase in fracture toughness [48]. This mechanism was corroborated in Figure 14(c), which shows nanotubes dangling from epoxy separated from carbon fiber (as indicated by white ellipse). In Figure 14(c), the dangling nanotubes were either broken or pulled out of the matrix.

The images of fracture surfaces of the pristine nanotubes sample indicated fracture mechanisms which might have led to the small increase in fracture toughness. As indicated by SEM images in Figure 13 and 14, the crack propagated through the nanotube network leaving some nanotubes on the carbon fibers (Figure 14(a)) as well as on the matrix (Figure 14(b)). Disentanglement of nanotube bundles and broken or pulled out nanotubes as seen in Figure 14(c), indicated mechanisms for energy dissipation, that could lead to increased fracture toughness. Second, the pristine nanotubes were mostly found on the surfaces of either the fiber or the matrix indicating poor bonding. This poor affinity could be a result of the absence of a chemical functional group on the pristine nanotubes. Therefore, the effect of pristine nanotubes on the matrix properties might be insignificant. This observation supports the DCB results, from which it has been observed that the load–displacement curves follow approximately same shape as base laminate without nanotubes. Only one curve shows unstable crack extension of about 20 mm and may be an outlier due to uneven

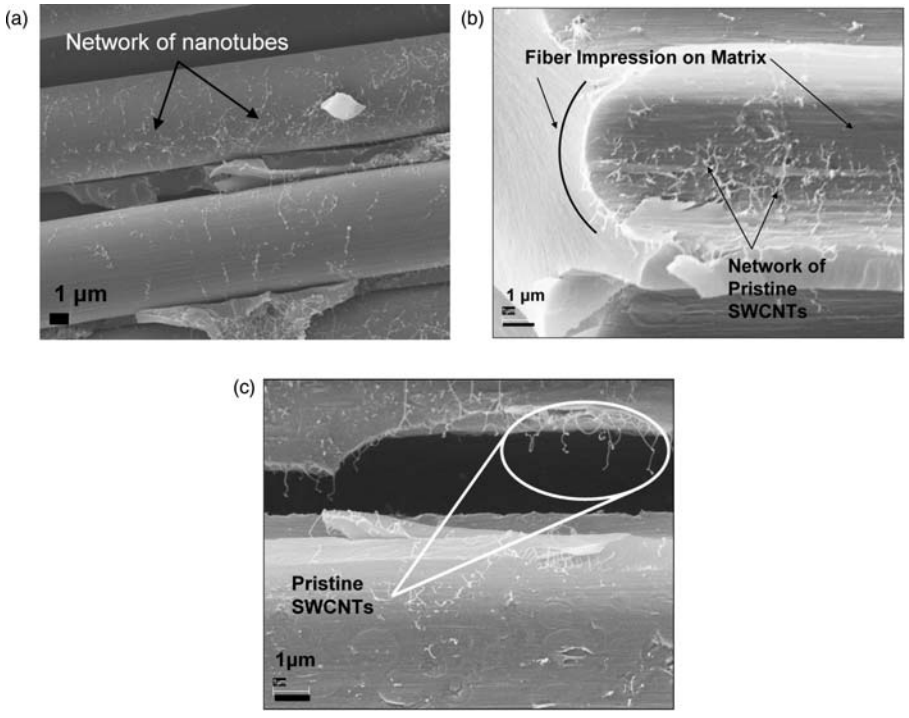

Figure 14. SEM images of observed mechanisms showing pristine SWCNTs: (a) on carbon fibers forming network, (b) on matrix impression after fiber debonded from the surface showing poor fiber–matrix bonding, and (c) pulled out/ broken CNTs after crack bridging.

distribution of nanotubes resulting in enough interaction of a cluster of nanotubes with epoxy matrix to delay the crack propagation.

Figure 15 includes low magnification images for sample 2P3, which contains the functionalized nanotubes. The images in Figure 15(a) and (b) show the delamination initiation edge. Figure 15(c) includes an image taken 10 mm from the delamination initiation, and Figure 15(d) is taken at 30 mm from the delamination initiation. These images, like those for the samples with pristine nanotubes, show some broken or pulled out carbon fibers at the surface. However, these images also show bands of epoxy which span large portions of the images which have smooth surfaces. The presence of the functionalized nanotubes therefore facilitates a combination of adhesive failure at the fiber–matrix interface, and cohesive failure through the epoxy as shown in the images. Figure 15(d) indicating smooth matrix surface at approximately 30 mm from the delamination initiation edge for specimen 2P3 confirms brittle crack propagation as observed from Figure 10 representing sudden decrease in G_{Ic} and large delamination extension.

Figure 16 includes SEM images at high magnification of a specimen with functionalized nanotubes. Areas in which the matrix material remains on the fiber after the crack passed through the matrix are visible in Figure 16(a). This intact fiber–matrix interface is further evidence of cohesive failure. It has been observed in Figure 16(b) and (c), that the functionalized nanotubes are sparsely scattered on the fibers as well as matrix, indicating inhomogeneous distribution. In fact, very few nanotubes were visible on the fracture surface, and not in the form of an extensive network as in the case of samples with pristine nanotubes. Due to the chemical functionalization process, the nanotubes were typically cut short in length due to acid reaction, as well as debundled into smaller ropes of nanotubes. In Figure 16(b), a nanotube-rich region has been observed between two carbon fibers. Here, the nanotubes were spread throughout the epoxy matrix between the fibers indicating better dispersion of nanotubes and compatibility with the epoxy matrix. It also indicated that the carbon fiber–epoxy matrix bonding has been improved by the presence of nanotube-rich interphase region. Another location that the nanotubes are visible is between the carbon fiber and the matrix (Figure 16(c)) where their ends are visible protruding out from the edge of the epoxy.

In Figure 16(c) and (d), microcracks are initiated near nanotube-rich areas which are very different from the rest of the fracture surface where nanotubes

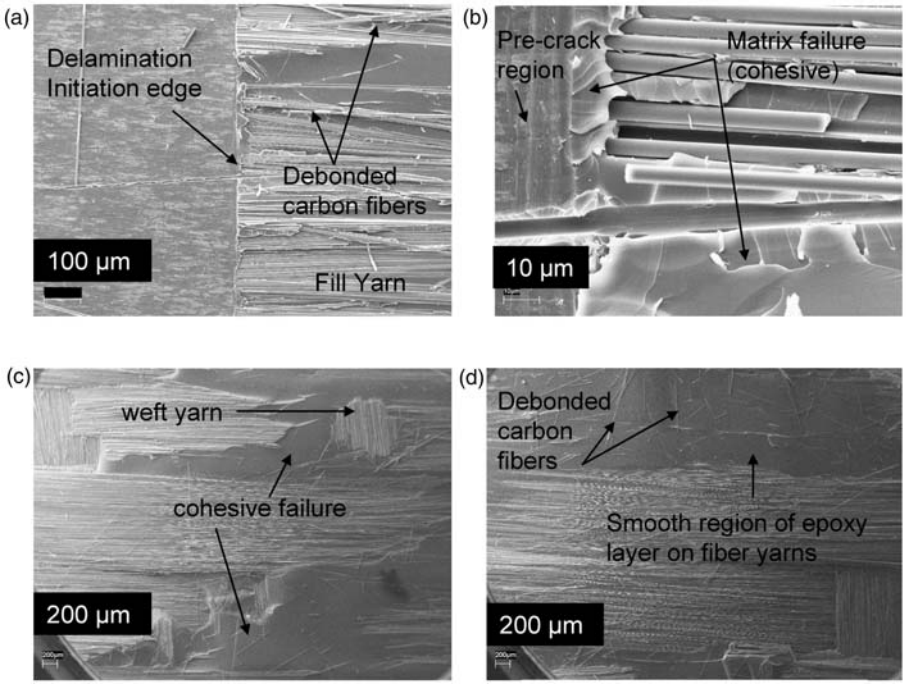

Figure 15 Low magnification SEM images of the delamination surface from the panel with silane functionalized SWCNTs: (a,b) 0 mm (delamination initiation), (c) 10 mm from delamination initiation, (d) 30 mm from delamination initiation.

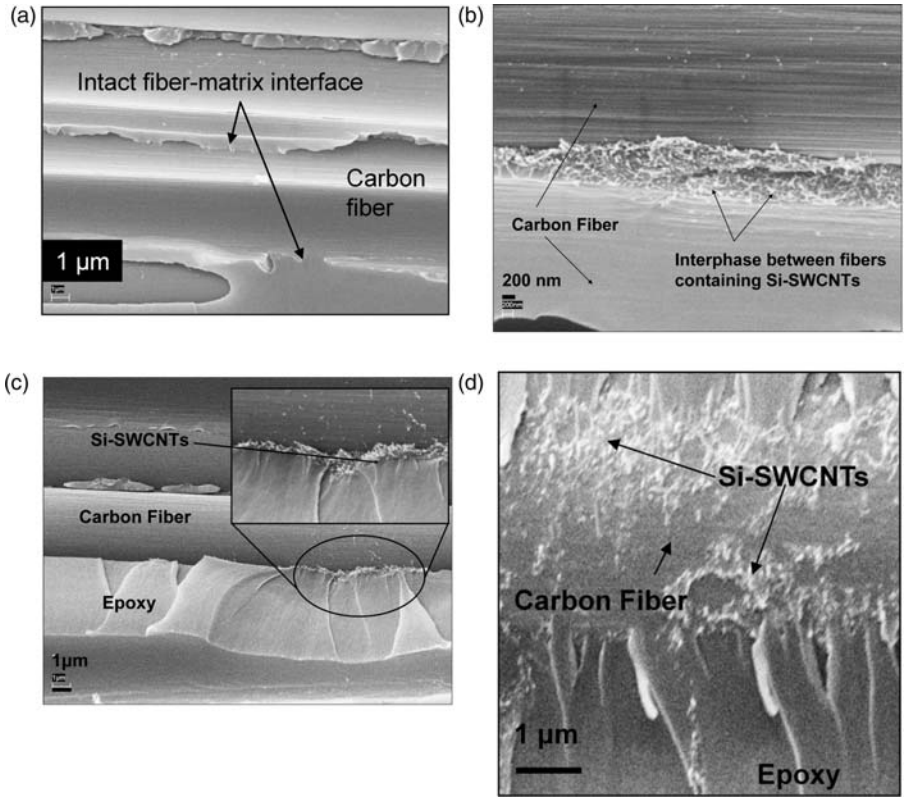

Figure 16 SEM images of observed mechanisms showing: (a) remnant matrix on the ply surface, (b) functionalized SWCNTs forming an interphase region between two carbon fibers, (c) enhanced fiber–matrix bonding where nanotubes are present, and (d) micro-cracks pattern due to better bonding between matrix and carbon fiber as a result of silane functionalized SWCNTs.

were not present. Figure 16(b) and (d) indicating nanotube rich regions and better fiber–matrix bonding are taken from a region which is approximately 10 mm away from the delamination initiation edge for specimen 2P3. These images are taken from the vicinity of the peak G_{Ic} value just before large delamination extension. So these images can be correlated to the particular G_{Ic} (632 J/m^2) value corresponding to 9 mm of delamination extension for the same specimen 2P3 from Figure 10. This is the peak G_{Ic} value before the start of large delamination extension. These SEM results indicate that the presence of functionalized nanotubes resulted in better fiber–matrix bonding, which would require higher energy to break the bonds. Second, the silane functional group has better affinity toward epoxy matrix which might result in higher resistance to fiber pullout, absorbing more energy in the process. However, the functionalized nanotubes were sparsely distributed on the fabric surface which may be because of the absence of nanotube networks and hence easier transfer of these nanotubes to another plane through the separation between carbon fiber tows during resin transfer process under vacuum. Thus, the energy required to propagate the delamination through nanotube-rich areas of epoxy would be much higher than required for delamination propagation through areas without any nanotubes (along the surface of the carbon fibers or in matrix regions where there are no nanotubes).[48,49] This combination of failure mechanisms indicates possible explanation for the unstable delamination extension through 25–30 mm. Absence of these large unstable crack growths in the panels with pristine nanotubes indicates a more homogeneous distribution of long SWCNTs that could have helped in stabilizing the crack growth along with higher G_{Ic}. Similar indications were made by Tong et al.,[48] who developed a mechanistic model to show an increase in G_{Ic} by increasing nanotube length and density.

The pristine and functionalized nanotubes therefore have shown different failure mechanisms, resulting in large part from the level of compatibility with epoxy matrix and the level of dispersion. In short, it has been observed from the above fractographic analysis of delamination surfaces that pristine nanotubes could help in bridging cracks while functionalized nanotubes could provide better fiber–matrix bonding and therefore a more substantial amount of cohesive failure in addition to the adhesive failure observed for the pristine nanotubes.

Summary

The multi-scale laminates consisting of macro-scale woven plies of micron sized carbon fibers were produced using VARTM method with selective placement of nanoscale carbon nanotubes at the mid-plane of the laminate using the spraying technique. The initiation G_{Ic} did not show any significant change for the panels with pristine and functionalized nanotubes as compared to the panel without nanotubes. However, the specimens with functionalized nanotubes showed a large unstable crack growth mechanism(20–30 mm). The reasons for the large unstable crack growth were investigated using SEM fractography of the delamination surfaces. It was found to be due to modified fiber–matrix bonding at the location of functionalized nanotube-rich interphase regions which enhanced the bonding of silane functionalized nanotubes with the epoxy matrix and reducing the fiber–matrix debonding which is one of the energy dissipation mechanisms, as evident from the SEM images. The functionalization process also resulted in better dispersion of nanotubes; however, the distribution of functionalized nanotubes on the ply surface was inhomogeneous due to the out of plane transfer of disentangled nanotubes through the gaps in weave structure. The fiber bridging mechanisms were also suppressed as a result of smaller nanotube lengths due to this particular chemical functionalization process.

SEM images showed comparatively better coverage of the fabric ply by the pristine nanotubes, compared to the functionalized nanotubes. The entanglement of long pristine nanotubes can help in bridging cracks as observed from SEM fractography. The crack propagation was observed to be much more stable in these specimens as seen from the R-curves. A different functionalization with similar dispersion characteristics but which will have longer nanotubes forming entangled networks could help in getting homogeneous coverage of functionalized nanotubes on the ply.

It is also suggested that a synergistic combination of functionalized and nonfunctionalized nanotubes could provide a better approach in enhancing the interlaminar properties. The functionalized nanotubes could provide better resistance to delamination initiation due to enhanced adhesion properties of fiber–matrix interface while long pristine nanotubes could stabilize the crack propagation through crack bridging mechanism as observed in this study.

Acknowledgments

This study was supported by Texas Institute for Intelligent Bio-Nano Materials and Structures for Aerospace Vehicles funded by NASA Cooperative agreement no. NCC-1-02038. The authors would like to thank Mr James Baughman from Lockheed Martin for helping with SEM Fractography and Dr Roberto J. Cano from NASA-LARC for providing the carbon fiber material. We would also like to thank Dr Gary-Don Seidel for useful discussions on this article. This study was conducted while Dr Gates was the Branch Head of the DDTR Branch at NASA LaRC and his contributions in bringing the team together for this project were essential, in addition to his technical participation in this study. Authors would also like to thank Dr Edward Glaessgen for helping with the article review process at NASA.

References

1. Brunner AJ and Flueler P. Prospects in fracture mechanics of engineering laminates. *Eng Fract Mech* 2005; 72: 899–908.
2. Chou TW. *Microstructural design of fiber composites*. Cambridge: Cambridge University Press, 1992.
3. Daniel IM and Ishai O. *Engineering mechanics of composite materials*. New York: Oxford University Press, 1994.
4. Sela N and Ishai O. Interlaminar fracture toughness and toughening of laminated composite materials: a review. *Composites* 1989; 20(5): 423–435.
5. Tsai SW and Hahn HT. *Introduction to composite materials*. Stamford, Connecticut: Technomic Publishing Company, 1980.
6. Njuguna J and Pielichowski K. Polymer nanocomposites for aerospace applications: properties. *Adv Eng Mater* 2003; 5(11): 769–778.
7. Njuguna J, Pielichowski K and Alcock JR. Epoxy-based fibre reinforced nanocomposites. *Adv Eng Mater* 2007; 9(10): 835–847.
8. Jurf RA and Pipes RB. Interlaminar fracture of composite materials. *J Compos Mater* 1982; 16: 386–394.
9. Whitney J, Browning CE and Hoogsteden W. A double cantilever beam test for characterizing Mode I delamination of composite materials. *J Reinf Plast Compos* 1982; 1: 297–313.
10. O'Brien TK. Interlaminar fracture of composites. NASA TM 85768, 1984.
11. Choi NS, Kinloch AJ and Williams JG. Delamination fracture of multidirectional carbon-fiber/epoxy composites under Mode I, Mode II and mixed-mode I/II loading. *J Compos Mater* 1999; 33(1): 73–100.
12. Bekyarova E, Thostenson ET, Yu A, Kim H, Gao J, Tang J, et al. Multiscale carbon nanotube - carbon fiber reinforcement for advanced epoxy composites. *Am Chem Soc* 2007; 23: 3970–3974.
13. Bekyarova E, Thostenson ET, Yu A, Itkis ME, D F, Chou TW, et al. Functionalized single-walled carbon nanotubes for carbon fiber–epoxy composites. *J Phys Chem C* 2007; 111: 17865–17871.
14. Thakre PR, Lagoudas DC, Zhu J, Barrera EV and Gates, TS. Processing and characterization of epoxy/SWCNT/woven carbon fabric composites. In: *47th AIAA/ASME/ASCE/AHS/ASC structures, structural dynamics and materials conference*. Vol. AIAA 2006–1857, Newport, Rhode Island, 2006.

15. Thostenson ET, Li WZ, Wang DZ, Ren ZF and Chou TW. Carbon nanotube/carbon fiber hybrid multiscale composites. *J Appl Phys* 2002; 91(9): 6034–6037.
16. Veedu VP, Cao A, Li X, Ma K, Soldano C, Kar S, et al. Multifunctional composites using reinforced laminate with carbon-nanotube forests. *Nat Mater* 2006; 5(6): 457–462.
17. Wichmann MHG, Sumeth J, Gojny FH, Quaresimin M, Fiedler B and Schulte K. Glass-fiber-reinforced composites with enhanced mechanical and electrical properties benefits and limitations of a nanoparticle modified matrix. *Eng Fract Mech* 2006; 73: 2346–2359.
18. Garcia E, Wardle B, deVilloria R, Guzman de Villoria R, Wicks S, Ishiguro K, et al. Aligned carbon nanotube reinforcement of advanced composite ply interfaces. In: *49th AIAA/ASME/ASCE/AHS/ASC Structures, Structural Dynamics, and Materials Conference*, 7–10 April, vol. AIAA-2008-1768, Schaumberg, IL, 2008.
19. Garcia EJ, Hart AJ and Wardle BL. Long carbon nanotubes grown on the surface of fibers for hybrid composites. *AIAA J* 2008; 46(6): 1405–1412.
20. Yamamoto N and Wardle B. Electrical and thermal properties of hybrid woven composites reinforced with aligned carbon nanotubes. In: *49th AIAA/ASME/ASCE/AHS/ASC Structures, Structural Dynamics, and Materials Conference*, 7–10 April, Schaumberg, IL, 2008.
21. Kinloch AJ, Maxwell DL and Young RJ. The fracture of hybrid-particulate composites. *J Mater Sci* 1985; 20: 4169–4184.
22. Sohn MS and Hu XZ. Delamination behavior of carbon fibre/epoxy composite laminates with short fibre reinforcement. *Scr Metall Mater* 1994; 30(11): 1467–1472.
23. Shin S and Jang J. The effect of thermoplastic coating on the mechanical properties of woven fabric carbon/epoxy composites. *J Mater Sci* 2000; 35: 2047–2054.
24. Stevanovic D, Kalyanasundaram S, Lowe A and Jar PYB. Mode I and Mode II delamination properties of glass/vinyl-ester composite toughened by particulate modified interlayers. *Compos Sci Technol* 2003; 63: 1949–1964.
25. Kostopoulos V. Enhancement of the Mechanical Performance of Carbon Fiber Reinforced Epoxy Resin Composites by the Introduction of Carbon Nano-Fibers(CNF). In: *47th AIAA/ASME/ASCE/AHS/ASC Structures, Structural Dynamics, and Materials Conference*, Newport, Rhode Island, 2006, pp.1–10.
26. Frankland SJV, Harik VM, Odegard GM, Brenner DW and Gates TS. The stress-strain behavior of polymer-nanotube composites from molecular dynamics simulation. *Compos Sci Technol* 2003; 63(11): 1655–1661.
27. Gates TS, Odegard GM, Frankland SJV and Clancy TC. Computational materials: Multi-scale modeling and simulation of nanostructured materials. *Compos Sci Technol* 2005; 65(15–16): 2416–2434.
28. Hadjiev VG, Lagoudas DC, Oh ES, Thakre P, Davis D, Files BS, et al. Buckling instabilities of octadecylamine functionalized carbon nanotubes embedded in epoxy. *Compos Sci Technol* 2006; 66(1): 128–136.
29. Lagoudas DC, Thakre PR and Benzerga AA. Nanoindentation of CNT reinforced epoxy nanocomposites. In: *Sixteenth European Conference on Fracture (ECF16)*, Greece, 2006.
30. Odegard GM, Gates TS, Wise KE, Park C and Siochi EJ. Constitutive modeling of nanotube-reinforced polymer composites. *Compos Sci Technol* 2003; 63(11): 1671–1687.
31. Riddick JC, Frankland SJV and Gates TS. Multiscale Analysis of Delamination of Carbon Fiber-Epoxy Laminates with Carbon Nanotubes. In: *47th AIAA/ASME/ASCE/AHS/ASC Structures, Structural Dynamics, and Materials Conference*. Newport, Rhode Island, 2006, pp.1–12.
32. Seidel GD and Lagoudas DC. Micromechanical analysis of the effective elastic properties of carbon nanotube reinforced composites. *Mech Mater* 2006; 38(8-10): 884–907.
33. Thakre PR, Lagoudas DC, Zhu J, Barrera EV and Gates TS. Effect of functionalization and weight fraction of single wall carbon nanotubes on mechanical properties of epoxy nanocomposites. In: *International Conference on Computational and Experimental Engineering Sciences (ICCES)*. Chennai, India, 2005.
34. Thostenson ET, Ren ZF and Chou TW. Advances in the science and technology of carbon nanotubes and their composites: a review. *Compos Sci Technol* 2001; 61(13): 1899–1912.
35. Zhu J, PH Q, Rodriguez M, Margrave JL, Khabasheskhu VN, Imam AM, et al. Reinforcing epoxy polymer composites through covalent integration of functionalized nanotubes. *Adv Funct Mater* 2004; 14(7): 643–648.
36. Hammerand DC, Seidel GD and Lagoudas DC. Computational micromechanics of clustering and interphase effects in carbon nanotube composites. *Mech Adv Mater Struct* 2007; 14(4): 277–294.
37. Zhu J, Kim JD, Peng HQ, Margrave JL, Khabashesku VN and Barrera EV. Improving the dispersion and integration of single-walled carbon nanotubes in epoxy composites through functionalization. *Nano Letters* 2003; 3(8): 1107–1113.
38. Zhu J, Khabasheskhu VN, Imam AM, Crane R, Lozano K and Barrera EV. Processing and properties of polymer composites reinforced by functionalized SWCNTs. *Mater Sci Forum* 2005; 475-479: 1059–1062.
39. ASTM D 5528. *Standard test method for mode I interlaminar fracture toughness of unidirectional fiber-reinforced polymer matrix composites*. West Conshohocken, PA: ASTM.
40. de Morais AB, de Moura MF, Goncalves JPM and Camanho PP. Analysis of crack propagation in double cantilever beam tests of multidirectional laminates. *Mech Mater* 2003; 35: 641–652.
41. Paris I, Minguet PJ and O' Brien TK. Comparison of delamination characterization for IM7/8552 composite woven and tape laminates. In: Bakis CE (ed.) *Composite materials: testing and design fourteenth volume*, ASTM STP 1436. West Conshohocken, PA: ASTM International, 2003.
42. Hansen P and Martin R. DCB, 4ENF and MMB delamination characterisation of S2/8552 and IM7/8552. Technical Report N68171-98-M-5177. United States Army, EUROPEAN RESEARCH OFFICE OF THE US ARMY, London, England, 1999.

43. Hashemi S, Kinloch AJ and Williams JG. Corrections needed in doublecantilever beam tests for assessing the interlaminar failure of fibrecomposites. *J Mater Sci Lett* 1989; 8: 125–129.
44. Alif N, Carlsson LA and Boogh L. The effect of weave pattern and crack propagation direction on mode-I delamination resistance of woven glass and carbon composites. *Composites Part B* 1998; 29B: 603–611.
45. de Morais AB, de Moura MF, Marques AT and de Castro PT. Mode I interlaminar fracture of carbon/epoxy cross-ply composites. *Compos Sci Technol* 2002; 62: 679–686.
46. Richards Thissell W, Zurek AK and Addessio F. Mechanical properties and failure mechanisms of carbon fiber reinforced epoxy laminated composites. In: *AIP Conference Proceedings*, 2006, Vol. 370, pp.551–554.
47. Martin RH. Delamination characterization of woven glass/polyester composites. *J Compos Technol Res* 1997; 19(1): 20–28.
48. Tong LY, Sun XN and Tan P. Effect of long multi-walled carbon nanotubes on delamination toughness of laminated composites. *J Compos Mater* 2008; 42(1): 5–23.
49. Gojny FH, Wichmann MHG, Kopke U, Fiedler B and Schulte K. Carbon nanotube-reinforced epoxy-composites: enhanced stiffness and fracture toughness at low nanotube content. *Compos Sci Technol* 2004; 64(15): 2363–2371.